Current Driven Instabilities of an electromagnetically accelerated plasma*

88-042

E.Y. Choueiri**, A.J. Kelly† and R.G. Jahn‡
Electric Propulsion Laboratory
Princeton University
Princeton, NJ 08544

Abstract

A plasma instability that strongly influences the efficiency and lifetime of electromagnetic plasma accelerators has been quantitatively measured . Experimental measurements of dispersion relations (wave phase velocities), spatial growth rates and stability boundaries are reported. The measured critical wave parameters are in excellent agreement with theoretical instability boundary predictions . The instability is current driven and affects a wide spectrum of longitudinal (electrostatic) oscillations . Current driven instabilities, which are intrinsic to the high-current-carrying magnetized plasma of the MPD accelerator, were investigated with a kinetic theoretical model based on first principles. Analytical limits of the appropriate dispersion relation yield unstable ion acoustic waves for $T_i/T_e << 1$ and electron acoustic waves for $T_i/T_e >> 1$. The resulting set of non-linear equations for the case of $T_i/T_e = 1$, of most interest to the MPD thruster Plasma Wave Experiment, was numerically solved to yield a multi-parameter set of stability boundaries. Under certain conditions, marginally stable waves travelling almost perpendicular to the magnetic field would travel at a velocity equal to that of the electron current. Such waves were termed "current waves". Unstable current waves near the upper stability boundary were observed experimentally and are in accordance with theoretical predictions. This provides the first unambiguous proof of the existence of such instabilities in electromagnetic plasma accelerators.

I. Introduction

The electromagnetic acceleration of plasmas is a process that is most prone to current driven instabilities.

In accelerating a plasma by electromagnetic means, kinetic energy is invested in the electrons from the electromagnetic field. This energy is then imparted to the plasma by means of collisions. Inelastic exciting and ionizing collisions with neutrals are a necessary expenditure of energy that is needed to produce the plasma and ideally must be recovered as directed kinetic energy along with any excited internal and random translational modes of all heavy species through dethermalization (e.g. collisions with a nozzle wall or streaming along the lines of an applied magnetic nozzle) to achieve high efficiency. If a substantial recovery is made, we can talk of a hybrid electromagnetic/electrothermal accelerator. Dethermalization in these high power devices where the plasma is highly ionized is complicated by the associated non-equilibrium rate processes. The realization of a hybrid accelerator is a current research problem. On the other hand, for a purely electromagnetic device it would be tolerable to accept that all random and internal modes stay frozen, if thermalization is kept to a minimum i.e one would like to pay just the ionization price with the smallest possible expenditure in heating. If this was the case, a high efficiency purely electromagnetic accelerator would indeed be possible since at high power operation both the ionization and joule heating (classical binary collisional heating) expenditures are modest compared to the useful work done by the electromagnetic force. In practice, however, it is invariably found that the efficiency at the highest powers does not exceed 40% indicating that a major dissipative process other than collisional heating is in operation. This discrepancy is not much alleviated even if electrode power losses are taken into account. Several related anomalies become apparent when experimental data obtained with high power electromagnetic accelerators are reviewed (see refs. 1, 2 and 3 for instance)

1. considerably higher ion temperature than would be expected from purely collisional thermalization (especially near the anode)

2. electron temperature weakly dependent on operating conditions or geometry (2 to 3 eV)

3. high Ionization rates that cannot be accounted for by classical thermal ionization.

4. presence of doubly ionized species with electron temperature not exceeding 3 eV

5. measurements of radiation losses (primarily line-line) substantially higher than what could be accounted for on classical grounds (ref. 2)

6. presence of thin ionization fronts across which strong jumps in ionization levels occur

7. presence of suprathermal electrons (ref. 2)

8. enhanced component heating, evaporation and erosion.

9. pronounced peaks in local electric fields fluctuation spectra

10. a drastic decrease in the plasma conductivity from classical levels

All the above phenomena can be shown to be the manifestation of plasma turbulence (nonlinear plasma instabilities) (refs. 3 and 4) . In these references the nonlinear wave theories start from the assumption that the instability is current-driven since these are known to be the most explosive and to lead to enhanced ionization, strong turbulent heating and anomalous resistivity. It is calculated from these theories, for instance, that the fraction of energy that goes into turbulent heating of ions (raising T_i) is a considerable portion of the accelerator input energy. It is also demonstrated that the nonlinear instabilities are in full effect even at low values of the total current J (for a fixed mass flow rate) and that the very processes of ionization and heating are dominated by the turbulence. When the accelerator's plasma becomes effectively fully ionized, the disappearance of wave damping collisions with neutrals frees the low frequency part of the spectrum (typically 200 to 500 khz for an argon plasma) to be current-driven unstable thus leading

* This research is supported by the National Aeronautics and Space Administration under contract NASA-954997 as well as grants from Hercules Aerospace, Rocket Research Inc. and DOE/Princeton Plasma Physics Laboratory.

** Graduate Student.
† Senior Research Scientist, Member AIAA.
‡ Professor of Aerospace Sciences, Fellow AIAA.

to an accentuation in the manifestation of the anomalies listed above. This would happen in the neighborhood of $\xi = 1$ (with $\xi \equiv J/J_{fi}$ where J_{fi} is the total current through the accelerator at the condition of full ionization and is defined in refs. 5 and 6).

If one compares the typical current velocities reached by the electrons for nominal accelerator conditions, to the ion thermal and natural velocities (c.f. figure 12.c) one soon realizes that an instability free electromagnetic plasma accelerator is highly unrealistic. This fact has long been recognized by soviet plasma physicists working on the MPD accelerator. Aref'ev (ref. 4), for instance emphasizes that the notion of non-turbulent electromagnetic plasma acceleration is contradictory.

Since these instabilities have a strong impact on both efficiency and lifetime of accelerators they are the subject of detailed studies at Princeton.

In this paper, we demonstrate the existence of the current driven instability mechanism through data obtained from an experiment that was specifically staged to measure unstable waves in their linear stage of growth. A kinetic model is used to interpret the data and identify the wave modes and instability mechanism.

II.Theory

II.a. Mathematical Model

In ref. 6 we treated the case of linear electrostatic waves in a current-carrying homogeneous and unmagnetized collisional plasma. At that time no clear experimental data on the nature of waves and instabilities in the MPD accelerator plasma were at hand. The Plasma Wave Experiment (PWX) described in section III has since yielded a quantitative database concerning waves and instabilities which helped refine the assumptions of the theoretical model. The assumptions made in the theory discused below are justified for a large range of the experimentally measured waves. Most importantly, the experiment was staged such that the effects of non-homogeneities and collisions with heavy species, could indeed be neglected while the magnetic field,, neglected in the previous theory, is retained in the present one. The effects of Coulomb collisions are not discussed in this paper so that the parametric dependences of the current driven instabilities are not clouded. They are treated in ref. (3).

The evolution of the particle distribution function $f_s(\mathbf{x},\mathbf{v},t)$ of species s in the six-dimensional phase space $(\mathbf{x},\mathbf{v})$ is assumed to obey the Vlassov equation :

$$\frac{\partial f_s}{\partial t} + \mathbf{v}\cdot\frac{\partial f_s}{\partial \mathbf{x}} + \frac{q_s}{m_s}\left[\mathbf{E}(\mathbf{x},t) + \mathbf{v}\times\mathbf{B}\right] \cdot \frac{\partial f_s(\mathbf{x},\mathbf{v},t)}{\partial \mathbf{v}} = 0 \qquad (1)$$

where m_s, q_s are the mass and charge of a particle of species s and $\mathbf{B}(\mathbf{x},t)$ and $\mathbf{E}(\mathbf{x},t)$ are the magnetic and electric fields respectively. The steady-state and homogeneous distribution function is denoted by f_s^o and defined as:

$$f_s^o(\mathbf{x},\mathbf{v}) = n_s^o F_s(v_\perp^2, v_z^2) \qquad (2)$$

where the subscripts $\perp$ and z denote components perpendicular and parallel to the magnetic field vector which is chosen arbitrarily to be aligned with the z axis . F_s is normalized such that:

$$2\pi\int_0^\infty v_\perp\, dv_\perp \int_{-\infty}^{\infty} F_s\, dv_s = 1 \qquad (3)$$

Moreover, the current density $\mathbf{j}(\mathbf{x},t)$ and the charge density $\rho(\mathbf{x},t)$ are related to the distribution functions by the following :

$$\mathbf{j}(\mathbf{x},t) = \sum_s q_s \int f_s(\mathbf{x},\mathbf{v},t)\,\mathbf{v}\, d^3\mathbf{v} \qquad (4)$$

$$\rho_s(\mathbf{x},t) = \sum_s q_s n_s(\mathbf{x},t) = \sum_s q_s \int f_s(\mathbf{x},\mathbf{v},t)\,\mathbf{v}\, d^3\mathbf{v} \qquad (5)$$

All quantities with spatial and temporal dependences, E, B, f_s, j and ρ are perturbed about their steady-state values (superscripted with o) by wave-like quantities (superscipted with a prime) and represented as Fourier-Laplace transforms such that for a perturbation A' of a generic quantity A we have :

$$A'(\mathbf{x},t) = \int e^{i\mathbf{k}\cdot\mathbf{x}}\, d^3\mathbf{k} \int \frac{e^{-i\omega t}}{2\pi i} A'(\mathbf{k},\omega)\, d\omega \qquad (6)$$

where k is the wave-vector and ω is the frequency Either ω or k is a complex quantity :

$$\mathbf{k} = \mathbf{k}_r + i\kappa \qquad (7)$$

$$\omega = \omega_r + i\gamma \qquad (8)$$

and γ and κ are the temporal and spatial growth rates respectively. In this nomenclature unstable (growing) waves correspond to a positive γ and negative κ. The Maxwell equations, linearized for small perturbations, relate the wave quantities in the following way:

$$\mathbf{k}\times\mathbf{E}' = \omega\mathbf{B}' \qquad (9)$$

$$i\mathbf{k}\times\mathbf{B}' = \mu_o\mathbf{j}' - i\omega\mathbf{E}' \qquad (10)$$

$$\mathbf{k}\cdot\mathbf{B}' = 0 \qquad (11)$$

$$i\mathbf{k}\cdot\mathbf{E}' = \epsilon_o\rho' \qquad (12)$$

where μ_o and ϵ_o are the permeability and permittivity of free space. For the special case of longitudinal (electrostatic) waves, we have $\mathbf{K}\times\mathbf{E}' = 0$ and the above equations can be manipulated to yield (see Stix ref. 7 for instance)

$$1 + \sum_s \frac{\omega_{ps}}{k^2} \sum_{n=-\infty}^{\infty} \int \frac{J_n^2(\mu_s)}{(\omega - n\omega_{cs} - k_z v_z)} \times \left[k_z \frac{\partial F_s}{\partial v_z} + \frac{n\omega_{cs}}{v_\perp}\frac{\partial F_s}{\partial v_\perp}\right] = 0 \qquad (13)$$

where ω_{ps} and ω_{cs} are the plasma and cyclotron frequencies of species s defined below, J_n is the Bessel function of the first kind of order n and μ_s a non-dimensional parameter that is a measure of how magnetized the particles are in the wave :

$$\omega_{Ps} = \left[\frac{q_s^2 \; n_s^o}{\epsilon_o m_s} \right]^{1/2} \; ; \; \omega_{cs} = \frac{q_s B^o}{m_s} \tag{14}$$

$$\mu_s = \frac{r_{c_s}^2 \; k_\perp^2}{2} \tag{15}$$

$$r_{c_s} = \frac{v_{t_s}}{\omega_{c_s}} \; ; \; v_{t_s} = \left[\frac{2T_s}{m_s} \right]^{1/2}$$

where we use the cyclotron radius r_{cs}, the thermal velocity v_{ts} and the temperature T_s of species s. Equation (13) relates the complex frequency ω of electrostatic oscillations to their wavenumber k (or wavelength). The dispersion relation, describes how a packet of waves is dispersed in the plasma as each of the components travels with a phase velocity $v_\phi = \omega/k$. This dispersion relation reduces to that of an unmagnetized plasma for $k_\perp = 0$ (i.e. propagation along the magnetic field). For propagation exactly perpendicular to the magnetic field ($k_z = 0$), the dispersion relation of ion or electron Bernstein waves is recovered. When solved for a real k the dispersion relation yields the frequency of the oscillations as well as their growth or damping rate. For a two-component plasma we can rewrite the dispersion relation above as a sum of the dielectric responses χ_s representing the contributions of free space, ions and electrons (with subscripts i and e referring to ions and electrons):

$$1 + \chi_e + \chi_i = 0 \tag{16}$$

We now consider only frequencies ω that satisfy the following criterion:

$$\omega_{ci} << \omega << \omega_{ce} \tag{17}$$

a condition shown in section III to be satisfied by the experiment. In other words we consider the ions to be unmagnetized in the waves, which is true when either:

$$k_\perp v_{ti} >> \omega_{ci} \tag{18a}$$

$$\text{or } (\omega_r, \gamma) >> \omega_{ci} \tag{18b}$$

is satisfied. Under these conditions the ion contribution in equations (13) and (16) becomes:

$$\chi_i(\omega, \mathbf{k}) = \frac{\omega_{pi}^2}{k^2} \int \frac{\mathbf{k} \cdot \partial F_i / \partial \mathbf{v}}{\omega - \mathbf{k} \cdot \mathbf{v}} d^3 \mathbf{v} \tag{19}$$

We shall furthermore specialize the dispersion relation to our particular case by first specifying that the steady-state equilibrium particle distribution functions are isotropic and Maxwellian:

$$F_s(v_\perp^2, v_z) = \left(\frac{m_s}{2\pi T_s}\right)^{1/2} e^{-\frac{m_s}{T_s}(v_\perp^2 + v_z^2)} \tag{20}$$

We shall also allow the electrons, which carry the current in the MPD accelerator, to have a relative drift velocity u_{de} with respect to the ions so that:

$$j = -e \, n_e^o \, u_{de} \tag{21}$$

We shall neglect the ion drift (or flow) velocity in the dispersion and the formalism would be applicable to a flowing plasma if the following criterion is satisfied:

$$\frac{\omega}{k} >> v_f \tag{22}$$

where v_f is the flow velocity. This criterion is amply satisfied in the experiment described below. Under the assumptions of isotropic, Maxwellian, electron current-carrying plasma χ_i and χ_e become after some algebra :

$$\chi_i(\omega, k) = \frac{\omega_{pi}^2}{k^2} \left[i + \zeta_i Z(\zeta_i) \right] \tag{23}$$

$$\chi_e(\omega, k) = \frac{k_\perp^2}{k^2} \frac{\omega_{pe}^2}{\omega_{ce}^2} \frac{1}{\mu_e} \left[1 + e^{-\mu_e} I_o(\mu_e) Z(\zeta_e) + \zeta_e \sum_{n \neq 0}^{\infty} e^{-\mu_e} I_n(\mu_e) Z\left(\frac{\omega - \mathbf{k} \cdot \mathbf{u}_{de} - n\omega_{ce}}{k_s v_{ts}}\right) \right] = 0 \tag{24}$$

where I_n is the modified Bessel function of the first kind of order n and of a generally complex argument, the complex parameters ζ_i and ζ_e are phase velocities non-dimensionalized by thermal velocities:

$$\zeta_i = \frac{\omega}{k v_{ti}} \quad \text{and} \quad \zeta_e = \frac{\omega - \mathbf{k} \cdot \mathbf{u}_{de}}{k_z v_{te}} \tag{25}$$

they appear as the arguments of $Z(\zeta_s)$ called the plasma dispersion function defined in the complex domain as:

$$Z(\zeta_s) = \frac{1}{\sqrt{\pi}} \int_{-\infty}^{\infty} \frac{e^{-t^2}}{t - \zeta_s} dt \tag{26}$$

The summation in equation (24) is over the electron cyclotron harmonics all of which except the zeroth order one can be neglected if :

$$u_{de} \lesssim v_{te} \tag{27}$$

a condition also respected by the experiment. The dispersion equation (16) can thus be finally written as:

$$1 + \alpha_e \left[1 + e^{-\mu_e} I_o(\mu_e) \zeta_e Z(\zeta_e) \right] + \alpha_i \left[1 + \zeta_i Z(\zeta_i) \right] = 0 \tag{28}$$

where the parameters α_s are defined :

$$\alpha_s \equiv \frac{k_\perp^2}{k^2} \frac{\omega_{ps}^2}{\omega_{cs}^2} \frac{1}{\mu_e} = \frac{2\omega_{ps}^2}{k^2 v_{ts}^2} = \frac{1}{k^2 \lambda_{ds}^2} \tag{29}$$

and are a measure of the wavelengths compared to the Debye lengths λ_{ds}. In our experiment both α_e and α_i are large on the order of 10^8 and 10^7 respectively. The major assumptions made so far along with the criteria for their justification are:

1. linear waves (see equation 68)

2. uniform plasma:

$$\frac{\omega}{k_\perp} >> \frac{T_s}{q_s B^o} \frac{d\ \ell n\ n^o}{dx}$$

$$\text{and } |k| >> \frac{d\ \ell n\ B^o}{dx} \ \& \ \frac{d\ \ell n\ n^o}{dx} \tag{31}$$

3. electrostatic oscillations: $\frac{\omega}{k} << c$ (32)

4. steady-state background: $\frac{\partial A^o}{\partial t} = 0$ (33)

5. plasma is collisionless in the waves:

$$\nu_{c_s} << \omega \tag{34}$$

6. ions unmagnetized in the waves:

$$\omega_{ci} << k_\perp v_{ti} \quad \text{or} \quad \omega_{ci} << (\omega_r, \gamma) \tag{35}$$

7. electron cyclotron harmonics are smeared:

$$u_{de} \lesssim v_{te} \tag{36}$$

8. wave phase velocities considerably larger than the flow velocity:

$$\frac{\omega}{k} >> v_f \tag{37}$$

The dispersion equation can now be solved to arrive at a parametric description of waves phase velocities, criteria for their instability and their growth rates. Analytical solutions of equation (28) are possible in the limits of very large and very small values of T_i/T_e. These two limiting cases are reviewed first. The first case leads to electron acoustic waves and the second gives ion acoustic waves. Both of these modes can be made unstable by the electron current. The magnitude of T_i/T_e that is necessary for the existence of each of these two modes is expressed in terms of the plasma and wave parameters. The plasma state and probe geometry of the experiment reported in this paper were such that neither of these two modes could be observed. Therefore the existence of current-driven instabilities could not be ascertained using these analytical solutions. This necessitated the treatment of the case of moderate T_i/T_e. Numerical solutions of equation (28) in the complex domain were thus undertaken. In this paper, for the sake of clarity, we shall only discuss the solutions near and at the instability boundaries which fortunately are sufficient to interpret the experimental data and demonstrate the existence of current-driven instabilities. For the complete solutions of equation (28) including substantial growth and comparison to experiments we refer the reader to Choueiri (ref. 3).

II.b Unstable Electron Acoustic Waves ($T_i/T_e >> 1$)

We first assume that T_i/T_e is sufficiently large so that :

$$|\zeta_e| = \left|\frac{\omega - k\cdot u_{de}}{k_z v_{te}}\right| >> 1 \tag{38}$$

$$\text{and } \zeta_i = \frac{\omega}{k v_{ti}} << 1 \tag{39}$$

The asymptotic expansions of the plasma dispersion function $Z(\zeta_s)$ for large and small arguments can therefore be used :

$$Z(\zeta_s) \approx -\frac{1}{\zeta_s} - \frac{1}{2\zeta_s^3} - \frac{3}{4\zeta_s^4}, \quad |\zeta_s| >> 1 \tag{40}$$

$$Z(\zeta_s) \approx -2\zeta_s + \frac{4}{3}\zeta_s^3 + i\sqrt{\pi}\exp^{-\zeta_s^2}, \ |\zeta_s| << 1 \tag{41}$$

Moreover we study only the case of long-wavelengths or equivalently the case of electrons strongly magnetized in the wave i.e. $\mu_e << 1$. For small arguments the modified Bessel function of the first kind and of the zeroth order can be approximated by:

$$e^{-\mu_e} I_o(\mu_e) \approx 1 - \mu_e \quad \text{for } \mu_e << 1 \tag{42}$$

and the dielectric responses of the ions and electrons, equations (23 and 24) become respectively :

$$\chi_e = \frac{k_\perp^2}{k_z^2}\frac{\omega_{pe}^2}{\omega_{ce}^2} - \frac{k_z^2}{k^2}\frac{\omega_{pe}^2}{\tilde{\omega}^2} + i\,2\sqrt{\pi}\,\frac{\omega_{pe}^2}{k^2 v_{te}^2}\,\frac{\tilde{\omega}}{k_z v_{te}}\,e^{-\left(\frac{\tilde{\omega}}{k_z v_{te}}\right)^2} \tag{43}$$

$$\chi_i = \frac{\omega_{pi}^2}{k^2 v_{ti}^2} + i\sqrt{\pi}\,\frac{\omega}{k v_{ti}}\left(\frac{\omega_{pi}^2}{k^2 v_{ti}^2}\right) \tag{44}$$

where

$$\tilde{\omega} = \omega - k\cdot u_{de} \tag{45}$$

Substituting the above expressions in equation (16) and solving for the phase velocity and the growth rate we get:

$$\frac{\omega}{k} = v_{se}\Lambda\cos\Theta + \sigma u_{de}\cos\phi \tag{46}$$

$$\gamma = -v_{se}\pi^{1/2} k\cos\theta \left\{ \left[\left[\frac{T_i}{T_e}\right]^{3/2} e^{-\Lambda^2 T_i/T_e} + \frac{v_{se}}{v_{ti}}\cos\theta \right] \Lambda^4 + \sigma\frac{u_{de}}{v_{ti}}\cos\phi\,\Lambda^3 \right\} \tag{47}$$

v_{se} is the electron acoustic velocity and is defined below along with the parameter Λ

$$v_{se} = \left(\frac{T_i}{m_e}\right)^{1/2}, \quad \Lambda = \left[1 + \frac{k_\perp^2 v_{ti}^2}{\omega_{ce}\,\omega_{ci}}\right]^{-1/2} \tag{48}$$

θ is the angle between the wave vector k and the magnetic field while ϕ is the angle between k and u_{de} (see figure 11 for the case of the MPD accelerator). σ is the sign of the dot product $k.u_{de}$. The instability boundary can be cast in terms of a threshold current velocity by setting γ to zero in the above equation to obtain:

$$u^*_{de} = \left[v_{ti} \left[\frac{T_i}{T_e}\right]^{1/2} e^{-T_i\Lambda^2/T_e} - v_{se}\cos\theta \right] \frac{\Lambda}{\sin\phi} \tag{49}$$

The above equations indicate that electron acoustic waves cannot be driven unstable (i.e. $\gamma>0$) by the current unless $\sigma<0$. Although these waves are of interest to the MPD plasma (since their instability threshold could be satisfied especially near the anode where the ions are hot) they are not relevant to the experimental case reported here since wave injection in PWX was always in the same sense as the current i.e. σ was always positive. Equations (46 and 47) are recoverable from Aref'ev (ref. 8) when assumptions (31) are made. Finally we recast the criterion $T_i/T_e>>1$ in more specific terms using (38 and 46):

$$\frac{T_i}{T_e} >> 1 + \frac{k^2 \cos^2\theta\, v_{ti}^2}{\omega_{ce}\,\omega_{ci}} \tag{50}$$

II.b Unstable ion acoustic waves ($T_i/T_e<<1$)

In parallel to the above case we assume that T_i/T_e is sufficiently small so that we have the following conditions

$$\zeta_i >> 1 \text{ and } |\zeta_e| << 1 \tag{51}$$

Using the asymptotic expansions (40) and (41) and proceeding as in the case above we obtain after some manipulations the phase velocity and growth rate for the more familiar ion acoustic waves

$$\frac{\omega}{k} = v_{si}\Lambda' \tag{52}$$

$$\gamma = -v_{si}(\pi)^{1/2} k\cos\theta \left\{ \left[\left[\frac{m_i}{m_e}\right]^{1/2} \left[\frac{T_e}{T_i}\right]^{3/2} e^{-\Lambda'^2 T_e/T_i} + \frac{v_{si}}{v_{te}\cos\theta} \right] \Lambda'^4 - \sigma \frac{u_{de}}{v_{te}} \frac{\cos\phi}{\cos\theta} \Lambda'^3 \right\} \tag{53}$$

v_{si} is the ion acoustic velocity and is defined below, along with Λ'

$$v_{si} = \left[\frac{T_e}{m_i}\right]^{1/2}, \quad \Lambda' = \left[1 + k^2 r_{ce}^2\right]^{-1/2} \tag{54}$$

Even though the growth or damping rate depends on the sense of propagation σ (as seen from equation 53), the threshold for instability is independent of σ, unlike the case of electron acoustic waves. This is readily seen by setting $\gamma = 0$ and solving for the critical current velocity at the boundary

$$u^*_{de} = v_{si} \left[1 + \Lambda' \cos \left[\frac{m_i}{m_e}\right]^{1/2} \left[\frac{T_e}{T_i}\right]^{3/2} e^{-\Lambda'^2 T_e/T_i} \right. \tag{55}$$

Finally, we recast the conditions (50) in closed form using equation (52) to give us more explicit criteria for the existence of these modes

$$\cos\theta > \left[\frac{m_e}{m_i}\right]^{1/2} \tag{56}$$

$$\frac{T_i}{T_e} << 1 + k^2 r_{ce}^2 \tag{57}$$

It is clear that in both limiting cases (equations (49) and (55)) the threshold on the current velocity is easily surpassed in the MPD accelerator where current velocities are, in many regions, two orders of magnitude larger than the ion thermal velocity. Although they emphasize the susceptibility of the plasma to current driven instabilities, the above analytical solutions of equation (28) cannot be used to interpret the results of PWX since the inequalities in (50) and (57) are not satisfied for the experimental conditions under which the instabilities were measured (cf. figure 12.a for plasma and probe parameters). We are therefore driven to consider the more complicated case of moderate T_i/T_e.

II.c The case of moderate T_i/T_e and the definition of "current waves"

We first rewrite equation (28) in more convenient form by noting that for most situations of interest to the experimentalist the measured wavelengths are considerably larger than the Debye length. From the definition at (29) this translates into a large α_s. As noted earlier, this condition is amply satisfied by PWX where α_e and α_i are on the orders of 10^8 and 10^7 respectively. Dividing equation (28) by α_i with $\alpha_i >> 1$we obtain from the real and imaginary parts the following set of nonlinear equations relating the complex variables ζ_e and ζ_i with T_i/T_e and μ_e as parameters:

$$\begin{aligned} &1 + \frac{T_i}{T_e}\left[1 + e^{-\mu_e} I_o(\mu_e)\zeta_e \,\mathrm{Re}\left\{ Z(\zeta_e) \right\} \right] + \zeta_i \,\mathrm{Re}\left\{ Z(\zeta_i) \right\} = 0 \\ &\frac{T_i}{T_e} e^{-\mu_e} I_o(\mu_e)\zeta_e \,\mathrm{Im}\left\{ Z(\zeta_e) \right\} + \zeta_i \,\mathrm{Im}\left\{ Z(\zeta_i) \right\} = 0 \end{aligned} \tag{58}$$

In order to numerically solve the above equations we need the following numerical tools. First, a plasma dispersion function generator in the complex domain for which the continued fraction representation of integral (26) was used (ref. 9). For $|\mathrm{Im}(\zeta_s)| < 1$ this method is weakly convergent and the Lanczos-τ method of Franklin (ref.10) was used instead. Second, the modified Bessel function of the first kind and of order zero with a generally complex argument was generated by means of an ascending series for small to moderate arguments and an asymptotic expansion for large arguments. Finally in order to find the roots of the nonlinear set of equations a specialized recursive Newton-Raphson algorithm was developed. Reference 3 has more details on these numerical tools.

The extensive solutions of these equations for substantial growth or damping can be found in ref.3 . In this paper, we present the more manageable set of solutions at the instability boundaries which is sufficient to identify the measured instability. For a marginally stable wave the plasma dispersion function (26) with a real argument x_s becomes

$$Z(x_s) = -e^{-x_s^2} \left[2\int_0^{x_s} e^{t^2} dt - i(\pi)^{1/2} \right] \tag{59}$$

and upon substitution in (58) we obtain the nonlinear set of equations at the instability boundary

$$1 + \frac{T_i}{T_e}\left[1 - 2e^{-\mu_e} I_0(\mu_e)\, x_e \int_0^{x_e} e^{t^2 - x_e^2} dt\right] + 2x_i \int_0^{x_i} e^{t^2 - x_i^2} dt = 0 \qquad (60)$$

$$\frac{T_i}{T_e} e^{-\mu_e} I_0(\mu_e)\, x_e\, e^{-x_e^2} + x_i\, e^{-x_i^2} = 0$$

where all the variables and parameters are non-dimensional. The real variables are

$$x_i = \frac{\omega}{k v_{ti}}, \quad x_e = \frac{\omega - k \cdot u_{de}}{k_z v_{ti}} \qquad (61)$$

In figure (1) the roots representing the non-dimensional phase velocity at the upper and lower limits of the instability are plotted versus the temperature ratio T_i/T_e with μ_e as parameter.

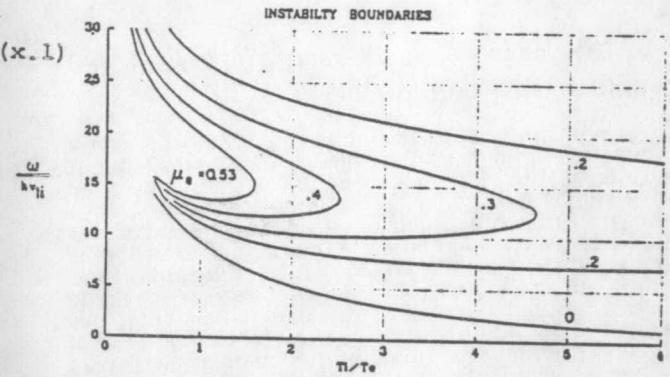

Figure 1. x_i at the boundary of instability as a function of the temperature ratio with μ_e as parameter

For a fixed μ_e there exists a cutoff temperature ratio for which the upper and lower boundaries merge. This singularity recedes to higher values of T_i/T_e as the electrons become more magnetized in the span of a wavelength i.e. as μ_e diminishes. For the extreme case of $\mu_e = 0$ the plot shows the lower instability boundary (for T_i/T_e up to 6) while the corresponding upper boundary is at infinity. For a fixed μ_e and for temperature ratios below the cutoff value, the curves indicate the highest and lowest phase velocities of the unstable oscillations. The existence and physical meaning of other roots are discussed in ref. 3 . Figure (2) is a similar plot for $|x_e|$. The curve for μ_e=0 is not shown here for the sake of clarity instead it is shown in figure (3) along with the curves for a moderately high μ_e.

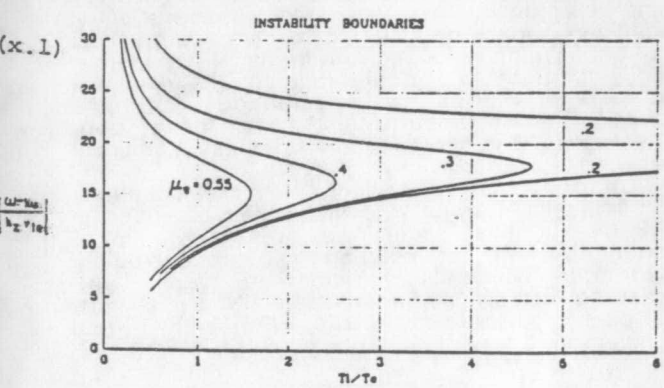

Figure 2. $|x_e|$ at the boundary of instability as a function of the temperature ratio with μ_e as parameter.

An interesting singularity happens when the curves for x_i and $|x_e|$ meet. This can be seen in figures (4) and (5) for the cases of upper and lower boundaries respectively.

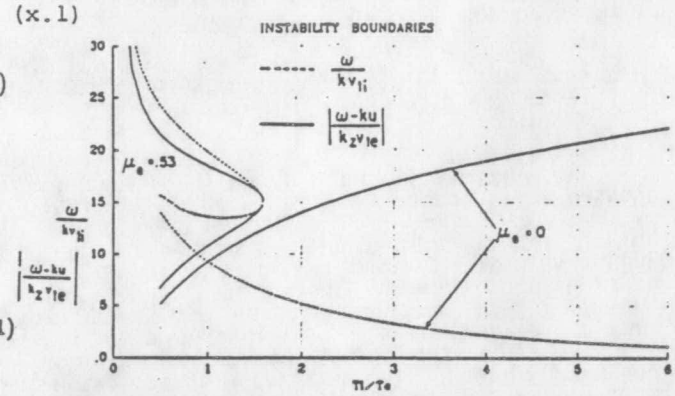

Figure 3. x_i and $|x_e|$ at the instability boundary as a function of the temperature ratio for the cases of nil and moderately small μ_e.

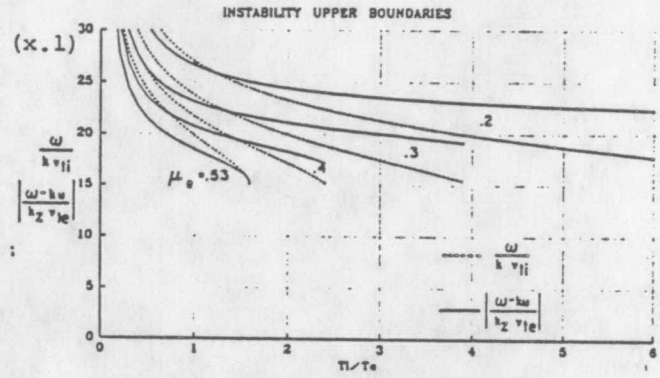

Figure 4. Solutions at the upper boundary showing current wave nodes (x_i=$|x_e|$).

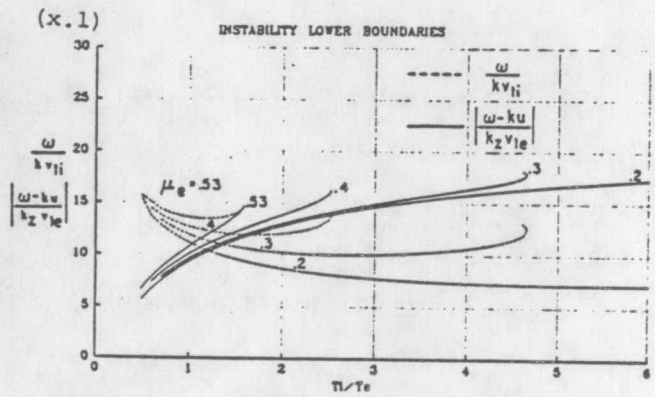

Figure 5. Solutions at the lower boundary showing current wave nodes (x_i=$|x_e|$).

Setting $x_i = |x_e|$ in (61) we get the phase velocity of the wave at the threshold of instability

$$\left(\frac{\omega}{k}\right)^* = \frac{u_{de}\cos\phi}{\cos\theta\left[\frac{T_e}{T_i}\right]^{1/2}\left[\frac{m_i}{m_e}\right]^{1/2} + 1} \qquad (62)$$

and for waves propagating almost perpendicular to the magnetic field or more explicitly at an angle θ

$$\cos\theta << \left[\frac{T_i}{T_e}\,\frac{m_e}{m_i}\right]^{1/2} \qquad (63)$$

their stability boundary is simply related to the current velocity

$$\left(\frac{\omega}{k}\right)^{*} \approx u_{de}\cos\phi \qquad (64)$$

Definition: We shall call "current waves" those waves that become marginally unstable when their phase velocity in the direction $\theta << \cos^{-1}(T_i m_e/T_e m_i)^{1/2}$ becomes equal to the current velocity component along the wave vector.

Conditions for the existence of current waves can be found by setting $x_i = |x_e|$ in equations (60) (see ref. 3 for a more detailed discussion). Graphically, the current wave branches can be seen by combining the two plots of figures (4) and (5) and connecting the nodes as shown in figure (6).

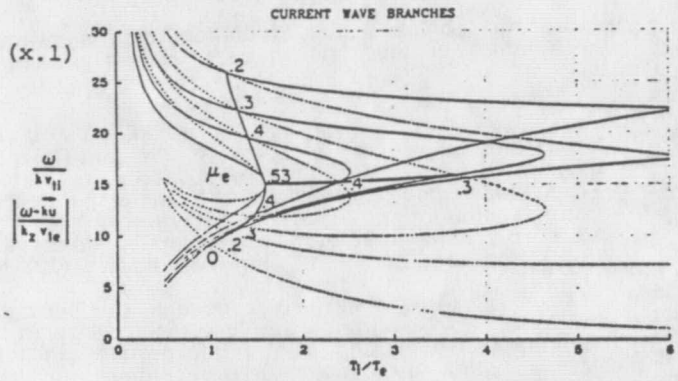

Figure 6. Branches of the "current wave" mode.

Aside from at the nodes there exists a branch of current waves at asymptotes where $x_i \rightarrow |x_e|$. In anticipation of the data of PWX where the experiment was staged in a nearly isothermal region of the plasma, the case of an isothermal plasma ($T_i/T_e = 1$) was solved for and the upper and lower instability boundaries are shown in figure (7). From this plot we conclude that current waves are to be expected in an isothermal plasma for $\mu_e \leq .1$ as seen from the upper boundary curve. At sufficiently low μ_e current waves are to be expected even if the plasma departs from the isothermal condition. In PWX, μ_e was typically on the order of 10^{-4} and indeed a current wave was observed and its instability measured as discussed in the next section.

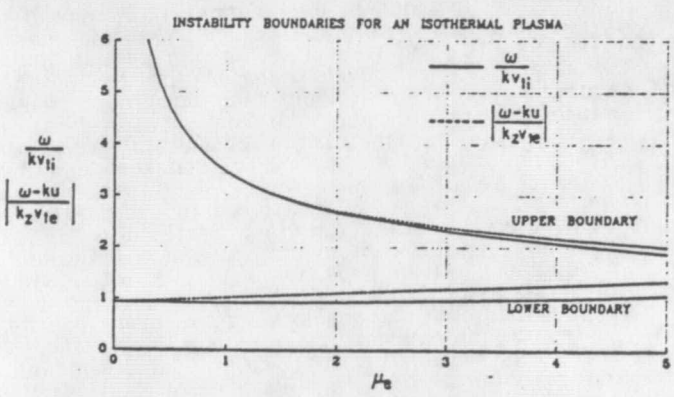

Figure 7. Boundary solutions for an isothermal plasma as a function of μ_e showing an asymptotic branch of current waves at small values of μ_e.

III. Experiment

The goal of the experiment is to supply measurements of plasma dispersion relations and spatial growth rates under conditions compatible with the theory so that the wave modes and instability mechanisms could be identified. Two types of measurements were made for each 1 msec pulse of the accelerator and are referred to as PWX and PCX. In PWX (Plasma Wave Experiment), wave parameters were measured such as dispersion relations (phase velocity spectra), intensity spectra, spatial growth rates, etc... PCX (Plasma Characterization Experiment) was concerned with the plasma parameters such as electron temperature, charged species density and magnetic field. The execution of these measurements was tailored such that all the above listed parameters were obtained during the quasi-steady part of the 1 msec pulse. Improvements on the hardware software and methods reported in ref. (5) are described below.

III.a Experimental set-up

The plasma accelerator selected for these studies was the Full-Scale Benchmark Thruster (FSBT) shown in figure (8). All experiments were conducted in a fiberglass tank 1.8 m in diameter and 4.8 m long maintained, by diffusion pumps at a pre-run pressure of about 10^{-5} torr. A 3000 μF pulse-forming network produces 1 msec long rectangular pulses driving a current through the accelerator of 3 to 30 kA. Argon is injected from the accelerator backplate at a mass flow rate of 6 g/sec. The probes for PWX and PCX are shown in figure (9). The PWX probes consisted of an emitter and receiver probe, each having two parallel cylindrical tungsten wires 5 mm long and .127 mm in radius. Low attenuation RG-217 coaxial cables were used to connect the probes to the diagnostics all of which were housed inside a Faraday cage. The current fluctuations of the probes were measured by Tektronix current probes and recorded on the two channels of a Nicolet digital recorder. Sampling rates of 200 nsec were selected for the results reported here corresponding to a Nyquist frequency of 5 MHz. The recorder is capable of storing 4096 samples. To prevent aliasing, a 3 MHz analog low pass filter was connected at each input. An analog spectrum analyzer (HP 8553b) with a 1.2 GHz ceiling RF section was kept on line with the emitter probe to provide real-time monitoring of the frequency spectrum. The frequency response of all the analog instrumentation was measured with the spectrum analyzer and found to be flat below the foldover frequency.

Since all plasma oscillations are in a steady saturation state, the dispersion relation of the plasma can only be obtained by monitoring the phase shift and amplitude variations of an injected wave packet. This injection was done by connecting the emitter (upstream) probe to a

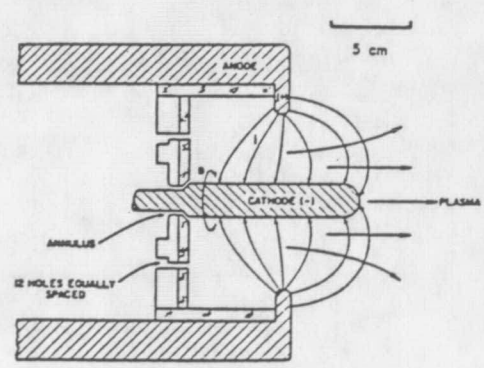

Figure 8. The Full Scale Benchmark Thruster FSBT.

Plasma Wave Driver which is an RF oscillator that can provide a harmonically rich spectrum of oscillations of about 20 volts peak-to-peak centered at the plasma potential. The receiver probe was held at a constant bias to draw ion saturation current. The PCX probe cluster consisted of an asymmetrical double Langmuir probe positioned parallel to the flow and a magnetic probe whose coil axis is positioned parallel to the local magnetic field. The Langmuir probe was chosen to be asymmetrical in order to increase the fraction of the electron distribution function that is sampled. The two cylindrical components were 7.62 mm long and .127 and .0635 mm in diameter. The bias voltage on the double probe was swept from -30 to +30 volts in about 50 µsec. The sweeping is triggered 100 µsec into the 1 msec pulse. The swept response of the current in the probe circuit was measured by a Tektronix P6041 Hall type current probe that has a frequency response of dc to 50 MHz. The probe circuit voltage was measured by a P6015 Tektronix voltage probe that also assured a capacitive decoupling of the floating Langmuir probe from the instruments. The measured probe characteristics were recorded on the two channels of another Nicolet digital recorder. The accelerator's terminal characteristics (voltage and total current), the output of the magnetic probe integrator and the various trigger pulses were recorded on a multi-channel Biomation 1015 digital recorder. In all up to 10 digital channels were in operation for each pulse. The data were transfered to an IBM 9000 micro computer for storage then up-loaded to the Princeton University IBM 3081 mainframe computer where all of the processing software is resident. Data processing and graphical manipulations are monitored on an interactive IBM 3277 GA workstation.

The PCX software has been described in (ref. 6) and various progress reports (ref. 11). The software processes the probe characteristics for an estimate of the electron temperature using asymmetrical double probe theory (ref.12). The charged species density is obtained from an interactive computerized version of Lam's Unified Theory (ref. 13). These data, along with other experimental inputs, are used to calculate various state, collisional and natural parameters of the plasma at the probe's location from established classical models. The probe theories validity parameters are then evaluated for consistency. The output is a list of the parameters and a set of scale ordering diagrams as later shown in figure (12).

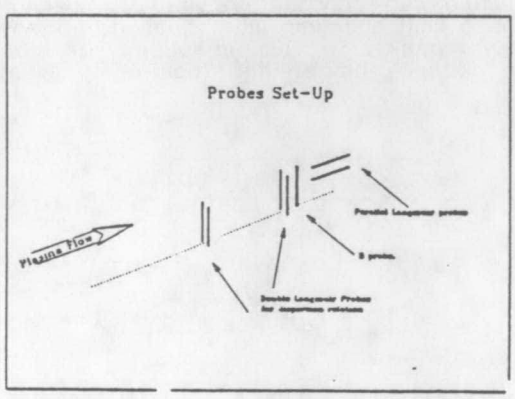

Figure 9. Probe cluster for PWX and PCX.

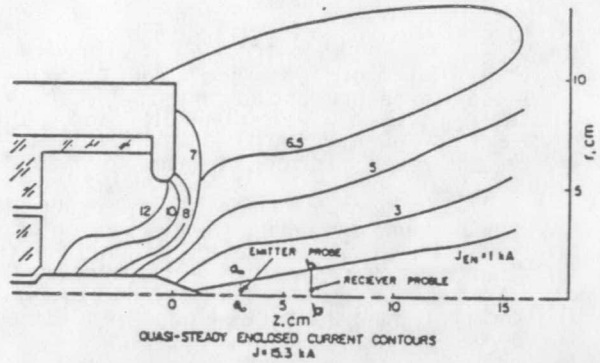

Figure 10. Enclosed current contour map showing the location of the emitter and receiver probes. (ref. 15)

The PWX software uses a Fast Fourier Transform algorithm to compute the phase and intensity spectra of the recorded oscillations. From these spectra and the probe cluster geometry, various spectra of parameters relevant to the study of instabilities can be estimated (see ref. (11) and are plotted as shown in figures (13) to (19).

A background clipping is done for all the data in order to eliminate the scatter due to the incoherent oscillations of the background plasma. This is done by clipping the background in the frequency domain below a certain attenuation. This process is completely unbiased as no pre-determined selection of peaks is made. Clipping could not help reduce the scatter when the peaks of the injected waves were swamped in the background noise . This type of severe deterioration to the signal-to-noise ratio happens when the accelerator's ξ is above .75 for the case where the emitter probe is 2 cm downstream of the tip of the cathode. A more powerful wave driver is needed to overcome this limitation. All PWX instrumentation tested negative for spurious phase shifts, attenuation or amplification for all frequencies up to 10 MHz.

III.b Experimental Results

The results reported here were obtained at ξ = .67 which, for the full scale Benchmark thruster device, corresponds to operation at 11.8 kA with 6 g/sec of argon. The probe cluster position is shown in figure (10) and was such that the emitter probe was at 1.7 cm downstream of the tip of the cathode. The axis joining the two probes which represents the direction of the measured wave vector, was parallel to the accelerator's axis of symmetry and at a small radial distance from the axis to avoid any r=0 singularities. The probe separation was a compromise to various conflicting effects among them: diagnostics sampling capability, frequency response, bandwidth of unstable waves and the assumption of uniform plasma. The probe cluster radial location was chosen near the cathode axis for two main reasons: 1) isothermal plasma conditions are most satisfied there as indicated by recent spectroscopic measurements of T_i and T_e (ref.14) and 2) the higher electron Hall parameters ($\Omega_e = \omega_{ce}/\nu_{ce}$) there (cf figure 10) permits simplification of equation (62) that is used to verify the wave mode at the boundary of instability. A high hall parameter implies that $u_y >> u_x$ in figure (11) and

the three vectors u_{de}, k and B become coplanar. This combined with the fact that for a self induced field, B and u_{de} are always perpendicular imply that (cf. figure 11)

$$\phi \approx \frac{\pi}{2} - \theta \quad (\Omega_e = \frac{j_y}{j_x} >> 1) \tag{65}$$

and the phase velocity of current waves at the stability boundary becomes simply

$$(\frac{\omega}{k})^* \approx u_{de} \qquad (\Omega_e = \frac{j_y}{j_x} >> 1) \tag{66}$$

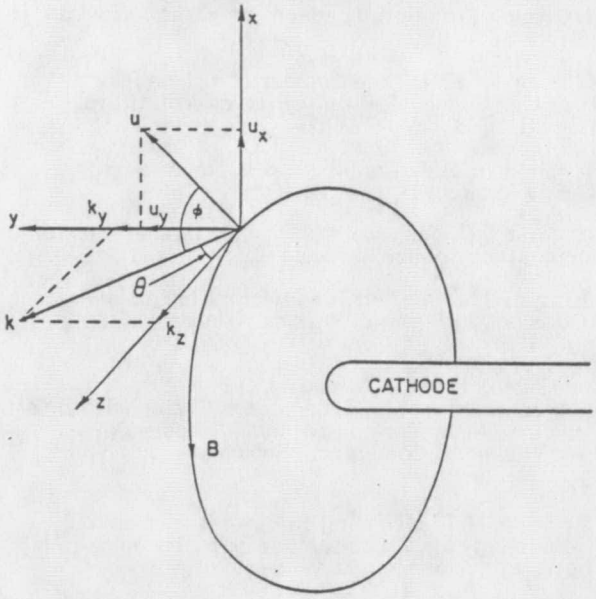

Figure 11. The k, u and B vectors in the accelerator plasma.

Figure (10) is a map of the current contour in the plasma that was constructed from magnetic probe measurements (ref. 15) with the FSBT at 15.3 kA and 6 g/sec (i.e. ξ = .87). This map can be used to estimate the average current velocity u_{de} in the experimental control volume bounded axially by the cross sections a-a and b-b of figure (10) where the probes are located. Assuming that the current density in the control volume scales linearly with the total current (this is a good assumption when the shape of the control volume bounded by the probes axial positions, the line of constant enclosed current and the symmetry axis stays similar with the total current which is the case for $\xi \leq 1$) the current velocity at an arbitrary ξ can be obtained from the following formula:

$$u_{de} = \frac{\xi J_o}{\xi_o e n_i \pi} \left[\frac{1}{r^2_{a-a}} + \frac{1}{r^2_{b-b}} \right] \tag{67}$$

where ξ_o and J_o are respectively the value of ξ and the magnitude of the nearest measured enclosed current line for the conditions under which the map was obtained, r_{a-a} and r_{b-b} are the radii to this line from the axis at the locations of the emitter and receiver probes respectively, e is the fundamental charge and n_i is the ion number density measured by PCX for the case in question. In this experiment we have ξ_o = .87 from the conditions of the map, r_{a-a} = .6 cm, r_{b-b} = 1.2 cm, J_o = 1 kA from figure (10), ξ = .67 and n_i = 2.21×10^{20} m^{-3} from the output of PCX (figure 12.a), thus yielding u_{de} = 120.2 km/sec.

The experiment conditions and the plasma parameters are shown in figure (12). In computing the various plasma parameters from the measured quantities, an isothermal plasma was assumed. An ionization fraction of 0.5 was also assumed for an overestimate of the frequencies of collisions with neutrals (the Saha value is .999) all of which where substantially lower than the measured wave frequencies. The local plasma flow velocity was estimated with three independent methods (ref. 11) at 5.83 km/sec.

Figures (13) to (18) show the results of the Plasma Wave Experiment. The time domain traces of the emitted and received signals are shown along with their corresponding power spectra in the frequency domain in figures (13) and (14). The cross spectrum and the phase spectrum are shown in figures (15 and 16). The data scatter in the phase spectrum was eliminated in figure (16) by background clipping at -24 db indicating that the scatter was indeed due to the incoherent plasma noise. The time delay spectrum was also plotted and with known probe separation was used to arrive at the phase velocity spectrum which in turn is equivalent to the dispersion relation plot (figures 17 and 18.a respectively). Finally, the clipped power spectra at the emitter and receiver were used with the known probe separation to arrive at the sought spatial growth rate spectrum of figure (18.b). In this plot negative values of the ordinate (the imaginary wave number) correspond to unstable waves (c.f. equation 5). Waves grow or get damped exponentially in space as $e^{-\kappa x}$ where κ is the ordinate of the spatial growth rate plots.

The spatial growth spectrum shows that the local plasma is unstable for oscillations between 1.7 and 2.7 MHz. This, to our knowledge, is the first direct experimental measurement of a convective plasma instability in electromagnetic plasma accelerators.

That the instability is an inherent trait of the plasma and not an effect of the active wave injection (i.e. that the injected waves are indeed linear) can be easily checked using the above plasma and wave parameters in the following criterion (ref. 16)

$$\frac{\omega}{k v_{ts}} \leq \frac{1}{(N k^2 \lambda^2_{ds})^2} = \frac{\alpha^2_s}{N^2} \tag{68}$$

where N is the number of plasma periods up to which linear waves can be assumed. This in essence a criterion for the smallness of the injected wave energy density compared to the plasma thermal energy density. The above criterion is amply satisfied in this experiment.

The strong damping at lower frequencies (cf. figure 18.b) is mainly due to collisional damping. Below 700 kHz no injected peaks survived in the background as can be seen from figures (14 and 15)

All spectra were therefore clipped at that frequency to avoid cluttering the plots with the low frequency incoherence. When the plasma becomes fully ionized (ξ=1) and the damping effects of collisions with neutrals are eliminated, it is to be expected that the lower part of the spectrum also becomes unstable.

Waves above the upper instability boundary were too damped to be observable in the narrow band between the boundary and the cutoff of the 3 MHz low pass filter. The location of the boundary (i.e. the frequency there) was verified to be insensitive to the nearness of the low pass cutoff and was thus a true plasma effect.

That we should expect a current wave mode is clear from the above theory. As can be seen from figure (12.b) the condition $\omega_{ci} << \omega << \omega_{ce}$ is amply satisfied for our experiment (ω between 1 and 3 MHz) and therefore the above theory can be invoked. The value of the parameter μ_e, easily computed from the above measured quantities, is less than 10^{-3} for all measured waves (the maximum wavenumber being 140 m^{-1}). This means that the electrons are strongly magnetized on the scale of a wavelength and from the theory above (cf figure 7 for instance), the asymptotic branch of current waves is to be expected. The wave phase velocity at the instability boundary would, according to (66), be very close to the electron current velocity u_{de} which for our case is 120.2 km/sec. This is indeed the case as shown in figure (19) where the theoretical prediction of the critical phase velocity is indicated by a threshold line on the phase velocity plot and equivalently a slope on the dispersion relation plot. It is seen that at the boundary of instability defined by the spatial growth data (i.e. 2.7 MHz) the phase velocity coincides with the predicted one. This proves that the measured instability is current driven.

IV. Conclusions

The major wave mode and instability mechanism inherent to the electromagnetic acceleration of a plasma are identified experimentally and theoretically. Current electrons which would ideally impart momentum to the plasma ions by the mildly dissipative process of Coulomb collisions create, in addition, an unstable distribution of energy that fuels disturbances into unstable exponential growth. Such current driven instabilities are notorious for dissipating energy in strongly enhanced ionization, turbulent heating of the ions to excessive temperatures, anomalous conductivity, component erosion and strong oscillations in the accelerator plasma limiting both efficiency and lifetime more than any other type of instability. In this paper, a theoretical study based on kinetic theory was used to interpret experimental measurements of an instability in the MPD thruster plasma. Phenomenological traits of the excited waves near their stability boundaries led to the unambiguous identification of the mechanism behind their instability.

Acknowledgments

We would like to thank Prof. T.H. Stix, Dr M. Ono, Dr. S. Zewben and Dr. T.K. Chu of the Princeton Plasma Physics Laboratory for their help and comments.

References

1. Artsimovich, L.A. (ed.), **Plasma Accelerators**, Mashinostroenie, Moscow, 1973.

2. Abramov, V.A., Vinogradova, A.K., Donstov, Y.P, Zavenyagi Y.A., Kovrov, P.E., Kogan, V.I. and Morozov, A.I. "Investigation of Electron Temperature and Plasma Discharge Between Coaxial Electrodes", Eighth Intl. conf. on Ionized Gases, Vienna, August-September 1967.

3. Choueiri, E. Y., "Instabilities of an Electromagnetically accelerated plasma", Ph.D. Thesis, Princeton University, 1988.

4. Aref'ev V.I., "Plasma Acceleration in crossed electric and magnetic fields", Sov. Phys. Tech. Phys., vol. 19, No.4 , pp 446 to 454. October 1974.

5. Choueiri, E.Y., Kelly, A.J., and Jahn R.G., "The Manifestation of Alfven's Hypothesis of Critical Ionization Velocity in the Performance of MPD Thrusters", 18th IEPC, Alexandria Va., AIAA-85-2037, 1985

6. Choueiri, E.Y., Kelly, A.J. and Jahn R.G., "MPD Thruster Plasma Instability Studies", 19th IEPC, Colorado Springs, Colorado, AIAA-87-1067, 1987.

7. Stix, T.H., **The Theory of Plasma Waves**, McGraw Hill, New York, 1962.

8. Aref'ev, V.I., "Current-Driven Instabilities in a Strongly Inhomogeneous Plasma, Parts I and II", Soviet Physics-Technical Physics Vol. 17, No. 7., pp. 1095 to 1107, January 1973

9. Fried, B.D. and Conte, S.D., **The Plasma Dispersion Function**, Academic press Inc., New York, 1961.

10. Franklin, R.N., "The Computation of the Plasma Dispersion Function", Plasma Physics, Vol. 10, pp. 805-808, 1968.

11. Choueiri, E.Y., Contributions to progress Reports, MAE 1776. from October 1986 to July 1988.

12. Swift, J.D. Schwar, M.J.R., **Electrical Probes for Plasma Diagnostics**, American Elsevier, N.Y., 1970.

13. Lam, S.H., "Unified Theory for the Langmuir Probe in a Collisionless Plasma", Physics of Fluids, Vol. 8, No. 1, Jan. 1965.

14. Heimerdinger, D.J., Kilfoyle, D.B., and Martinez-Sanchez M., "Experimental Characterization of Contoured Magnetoplasmadynamic Thrusters", 24th Joint Propulsion Conference, Boston Ma., July 11-13, 1988.

15. Boyle, M.J., "Acceleration Processes in the Quasi-Steady Magnetoplasmadynamic Discharge", Ph.D. Thesis, Princeton University, 1974.

16. Gentle, K.W. "Plasma Waves and Echoes", in **Methods of Experimental Physics: Plasma Physics, Part A**, H.S. Griem editor, Academic Press, New York, 1970.

I) GENERATION PARAMETERS

EXPERIMENT # EXPA

ACCELERATOR CURRENT	: 11.8 kA
ACCELERATOR VOLTAGE	: 60 Volts
ARGON MASS FLOW RATE	: 6 g/sec

II) PROBE PARAMETERS

PROBE AXIAL POSITION	: 5.18 cm from c.t.
PROBE RADIAL POSITION	: 0 cm from axis
PROBE(1) RADIUS AND LENGTH	: 0.0635 7.62 mm
PROBE(2) RADIUS AND LENGTH	: 0.127 7.62 mm
PROBE(1) AREA	: 3.053E^6 m^2
PROBE(2) AREA	: 6.131E^6 m^2
PROBES ASPECT RATIOS (1,2)	: 120 60
RATIOS OD Rp/Debye l (1,2)	: 81.35 163.7
KNUDSEN # (l/ mfp/Rp) (1,2)	: 12.89 6.444
VALIDITY PARA. FOR STATION-ART PLASMA PROBE THEORY	
PROBE(1)	: 4060 BASED ON Lp AND 33.83 BASED ON Rp
PROBE(2)	: 4060 BASED ON Lp AND 67.66 BASED ON Rp
ION SATURATION CURRENT (1)	: 0.16 Amp
ION SATURATION CURRENT (2)	: 0.344 Amp

III) GENERAL PLASMA PARAMETERS

ELECTRON TEMPERATURE	: 2.433 eV.
ION TEMPERATURE	: 2.433 eV.
CHARGED SPECIES DENSITY	: 2.21E20 m^-3
MASS DENSITY	: 0.00001464 kg/m^3
THERMODYNAMIC PRESSURE	: 1.291 torr
MAGNETIC PRESSURE	: 1.38 torr
BETA	: 0.9355
ATOMIC MASS	: 39.9 AMU
Ni/Ne	:7.2812%
MAGNETIC FIELD	: 0.0215 TESLA
ALFVEN VELOCITY	: 5012 m/sec
ION ACOUSTIC VELOCITY	: 242% m/sec
ELECTRON ACOUSTIC VELOCITY	: 654 Km/sec
EXHAUST VELOCITY	: 5829 m/sec
IONIZATION FRACTION	: 0.5
ELECTRON THERMAL VELOCITY	: 925 Km/sec (2-D) 1133 Km/sec (3-D)
ION THERMAL VELOCITY	: 3.428 Km/sec (2-D) : 4.198 Km/sec (3-D)
ELECTRON DEBYE LENGTH	: 7.805E^7 m
ION DEBYE LENGTH	: 7.805E^7 m
TOTAL DEBYE LENGTH	: 5.519E^7 m
ELECTRON PLASMA PARAMETER	: 792%
ION PLASMA PARAMETER	: 792%
TOTAL PLASMA PARAMETER	: 2801
LOG OF THE PLASMA PARAMETER	: 7.938

a PAGE -1- CHARACTERIZATION OUTPUT OF EXPERIMENT # EXPA

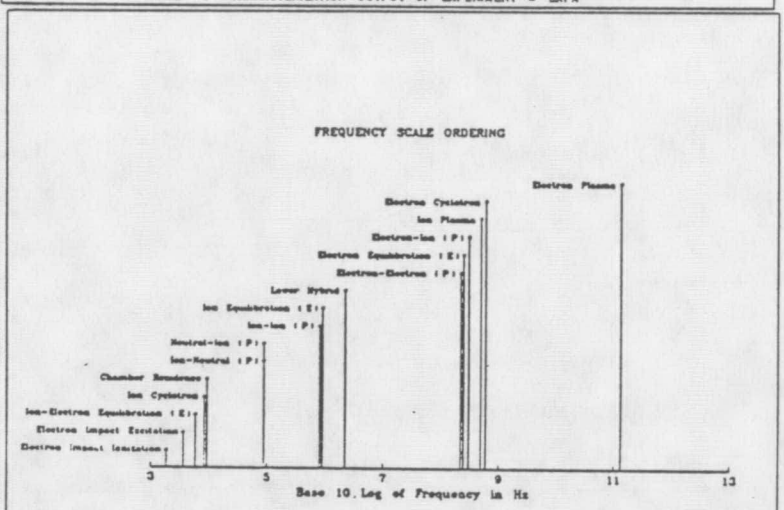

b PAGE -3- CHARACTERIZATION OUTPUT FOR EXPERIMENT # EXPA

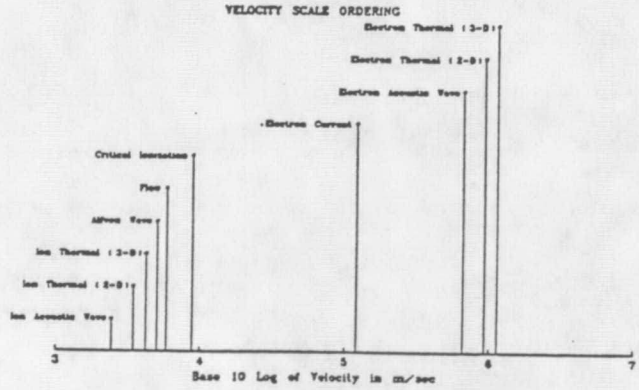

c PAGE -5- CHARACTERIZATION OUTPUT FOR EXPERIMENT # EXPA

Figure 12. Output of PCX for the present experiment: a) List of plasma parameters, b) frequency scale ordering diagram and c) velocity scale ordering diagram.

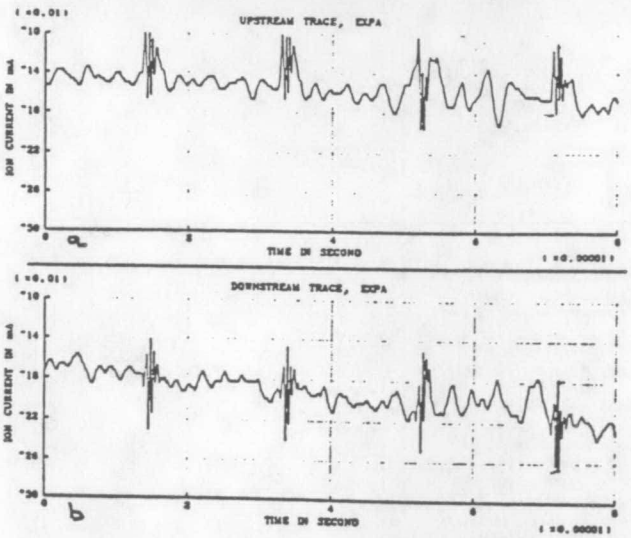

Figure 13. Time domain fluctuations of of injected waves at emitter and receiver.

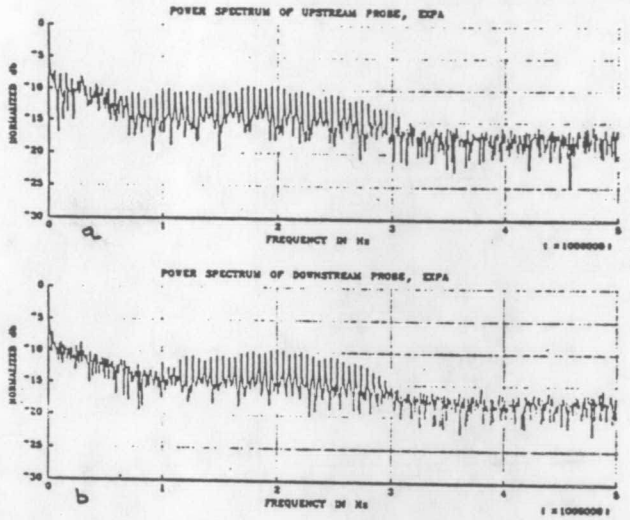

Figure 14. Frequency domain power spectra of injected waves at emitter and receiver (Doppler shifted)

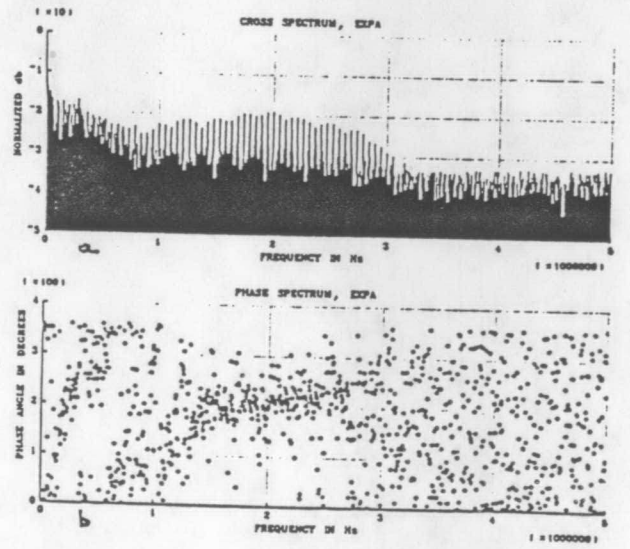

Figure 15. Unclipped power and phase cross-spectra (Doppler shifted)

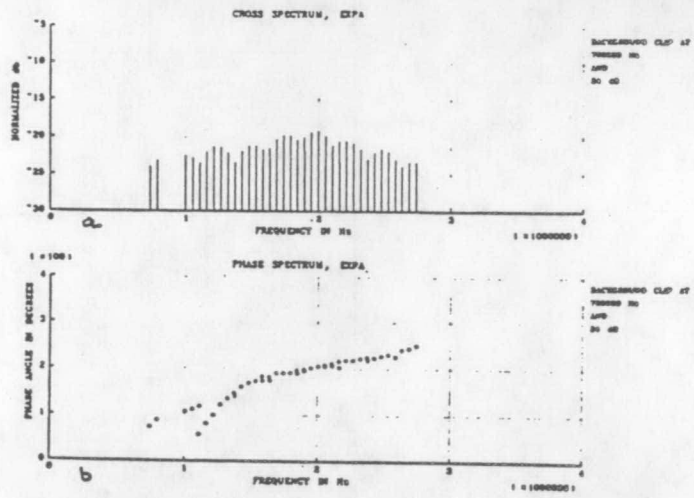

Figure 16. Same as figure 15, with background clipped at 700 kHz and -24 db (doppler shifted).

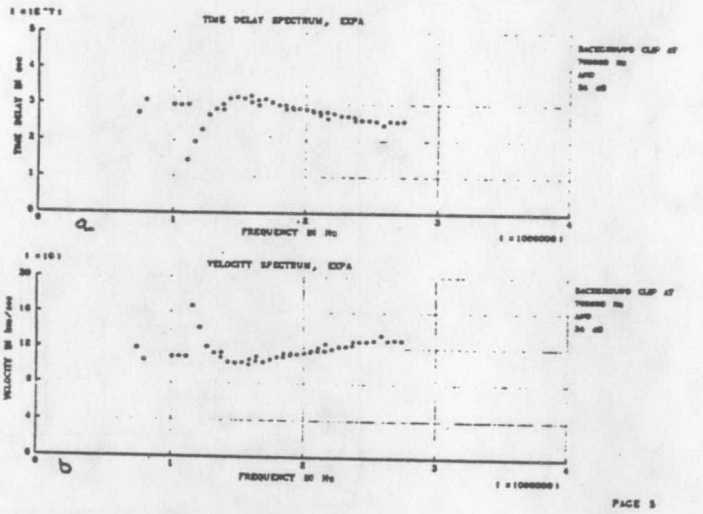

Figure 17. Time delay and phase velocity spectra (Doppler shifted).

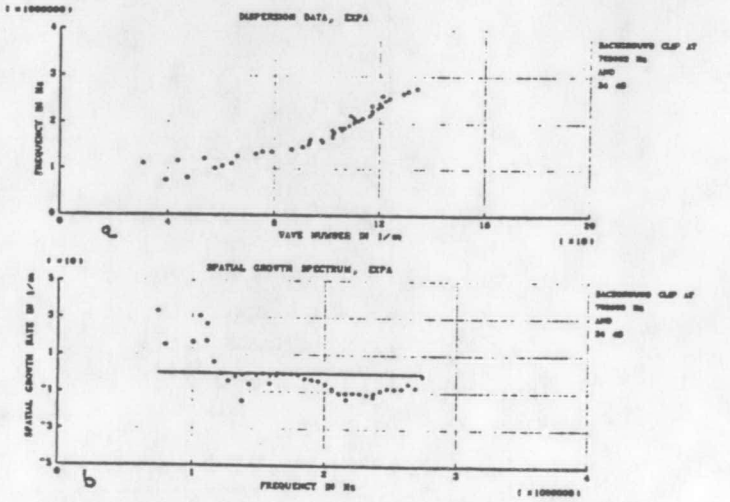

Figure 18. Dispersion relation and Stability plot (spatial growth spectra) showing instability, (Doppler shifted).

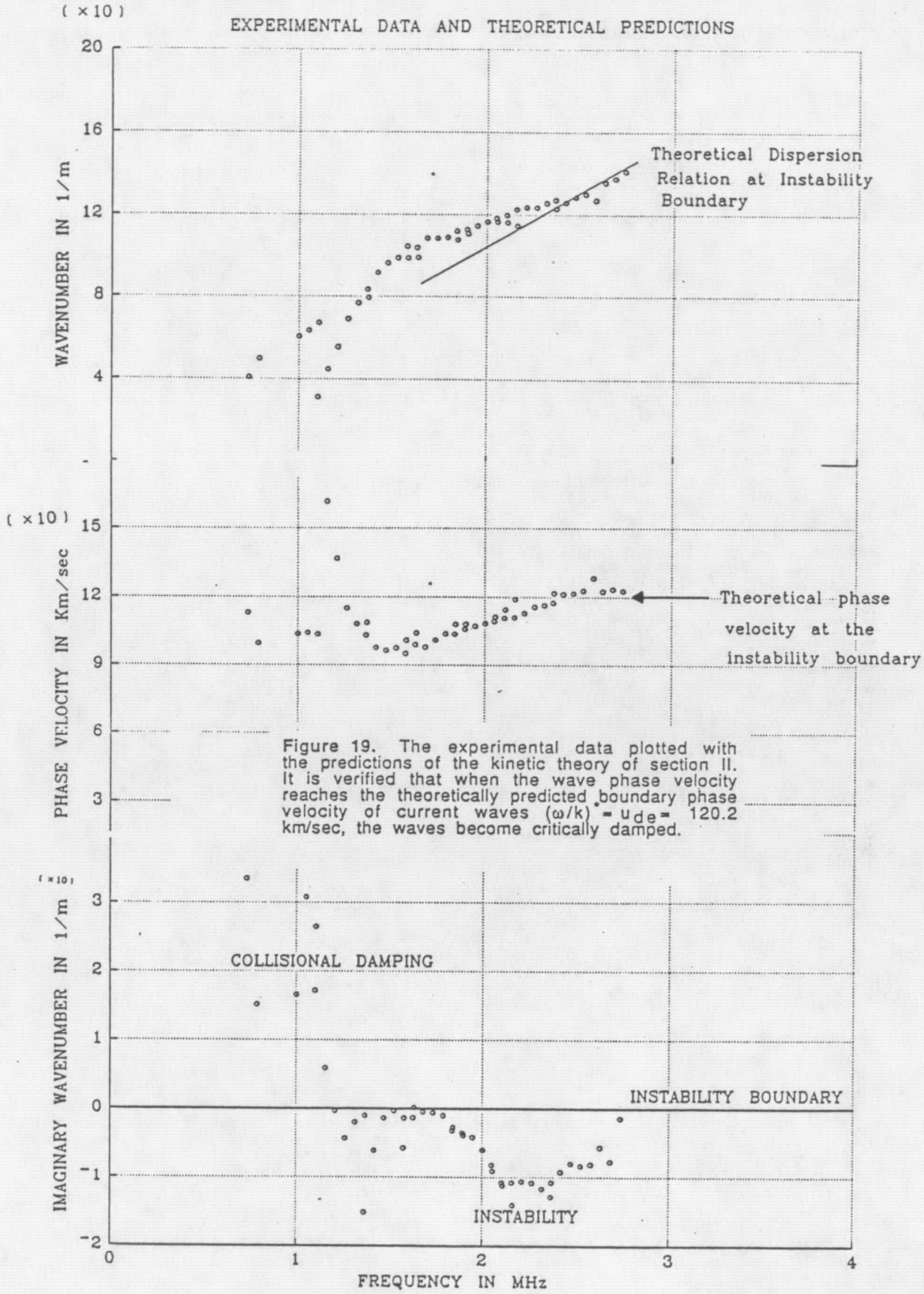

Figure 19. The experimental data plotted with the predictions of the kinetic theory of section II. It is verified that when the wave phase velocity reaches the theoretically predicted boundary phase velocity of current waves $(\omega/k) = u_{de} = 120.2$ km/sec, the waves become critically damped.